CleanMat

WILEY

CleanMat

RESEARCH ARTICLE OPEN ACCESS

KOH-Activated Pinecone Biochar for Efficient Chloramphenicol Removal From Aqueous Solutions

Xiaoran He[1,2] | Md. Amirul Islam[2] | Taibao Zhao[2,3] | Osama Eljamal[1] | Bidyut Baran Saha[2,3]

[1]Water and Environmental Engineering Laboratory, Interdisciplinary Graduate School of Engineering Sciences, Kyushu University, Kasuga, Japan | [2]International Institute for Carbon-Neutral Energy Research (WPI-I2CNER), Kyushu University, Fukuoka, Japan | [3]Department of Mechanical Engineering, Kyushu University, Fukuoka, Japan

Correspondence: Bidyut Baran Saha (saha.baran.bidyut.213@m.kyushu-u.ac.jp)

Received: 24 October 2024 | **Revised:** 8 January 2025 | **Accepted:** 22 January 2025

Funding: This work was supported by a scholarship from China Scholarship Council (No. 202307040018).

Keywords: adsorption | biochar | chloramphenicol removal | waste biomass | water pollution

ABSTRACT

The emerging pollutant chloramphenicol (CAP) is highly environmentally persistent and biotoxic, causing extreme environmental harm. This study investigates the removal of CAP from aqueous solutions using biochar derived from pinecones. The biochars were activated at 800°C using KOH with different mass ratios to the carbonized sample (2:1, 4:1, and 6:1). Among them, the biochar with a KOH ratio of 4:1 (PCK4-800) exhibits the highest pore volume (1.8 $cm^3\ g^{-1}$) and a specific surface area (3131.6 $m^2\ g^{-1}$). Batch experiments reveal that the CAP adsorption capacity of the biochar is positively correlated with its specific surface area. At pH 7, PCK4-800 achieves a removal efficiency of up to 92% for a 100 mg L^{-1} CAP solution using a dosage of just 0.1 g L^{-1}. This performance surpasses that of recently reported adsorbents. Kinetic and thermodynamic model fitting results indicate that chemical adsorption within a monomolecular layer dominates physical adsorption. The primary adsorption mechanisms involve pore filling and π-π interactions, while secondary mechanisms include electrostatic effects and hydrogen bonding. Thermodynamic parameters confirm that the adsorption process is endothermic and spontaneous. Moreover, the removal efficiency of PCK4-800 remains above 80% after five regeneration cycles. In summary, the high removal efficiency and excellent regeneration potential of PCK4-800 demonstrate its suitability as an effective adsorbent for antibiotic removal.

1 | Introduction

Antibiotics are extensively used in both human and veterinary medicine, playing a crucial role in modern healthcare systems [1]. However, the increasing use of antibiotics has led to the discharge of significant amounts of antibiotic-containing wastewater into aquatic environments. It has been found that 94 antibiotics have been detected in 25 aquatic environments across China, including groundwater, tap water, surface water, and seawater [2]. Many of these antibiotics are resistant to degradation and are usually discharged directly into water bodies as undecomposed drugs, causing significant risks to the ecological environment [3].

As an emerging wide-spectrum antibiotic, chloramphenicol (CAP) has been extensively studied due to its potential carcinogenicity and toxicity in humans and animals [4, 5]. CAP can cause aplastic anemia in many animals (e.g., cats, dogs, pigs,

Abbreviations: C_0, The initial CAP concentration mg L^{-1}; C_e, The equilibrium concentration of CAP solution mg L^{-1}; C_t, The CAP concentration at a predetermined time t mg L^{-1}; k_1, The PFO kinetic constant min^{-1}; k_2, The PSO kinetic constant g $(mg\ min)^{-1}$; K_D, The adsorption equilibrium constant L g^{-1}; K_F, The Freundlich constant L mg^{-1}; K_L, The Langmuir constant L mg^{-1}; m, the mass of the adsorbents g; q_e, The adsorption capacities at equilibrium mg g^{-1}; q_m, The maximum adsorption capacity of CAP mg g^{-1}; q_t, Removal capacity mg g^{-1}; q_t, The adsorption capacities at time t mg g^{-1}; R, The removal rate %; R, The universal gas constant J $(mol\ K)^{-1}$; t, A specific contact time s; T, Absolute temperature K; V, The volume of CAP solution L; ΔG^0, The Gibbs free energy kJ mol^{-1}; ΔH^0, The enthalpy change kJ mol^{-1}; ΔS^0, The entropy change J $(mol\ K)^{-1}$; PZC, The point of zero charge /.

etc.) and humans and is extremely lethal. CAP may inhibit bone marrow function in humans, and some individuals may vomit and have intestinal dysbiosis [6]. Its persistence in water bodies may lead to bioaccumulation and long-term harm to aquatic organisms [7]. These unfavorable impacts have led to an explicit ban on CAP addition to animal feed in many countries, including Australia, the United States, China, and some European countries [8]. Antibiotic pollution in Japan is primarily attributed to sources such as pharmaceutical manufacturing, improper disposal of unused medicines, and agricultural practices. Studies have detected the presence of antibiotics in rivers, wastewater, and soils, highlighting their persistence in the environment. Therefore, Japan enacted special laws and regulations for the environmental management of chemical substances in the 1960s and 1970s to promote the environmental risk control of new pollutants [9]. Moreover, studies have shown that CAP may be present in foodstuffs such as milk and eggs, so the Japanese government has established strict testing and regulatory standards for CAP residues in foodstuffs [10].

It is difficult to remove antibiotics completely through conventional wastewater treatment techniques, so developing an effective and sustainable remediation technique is necessary. Many studies have reported various techniques for antibiotic removal from water. The common ones are adsorption [11], advanced oxidation [12], membrane separation [13], photocatalysis [14] and biodegradation [15]. Among these, adsorption stands out among the techniques for removing antibiotics for its low cost, effectiveness, and accessibility. Additionally, it is effective in large-scale wastewater treatment [16]. Biochar is a common adsorbent for antibiotic removal as its surface has abundant oxygen-containing groups. There are abundant biomass raw materials in nature (e.g., agricultural wastes [17, 18], animal manure [19], municipal sludge [20]), and converting these wastes into highly efficient adsorbents is an effective way of resource utilization.

Pinecone (PC) is a common bio-waste in Japan. The high carbon content (42.64%) and low ash content (0.9%) make it particularly suitable for biochar production [21]. However, pristine biochar is often limited by its surface chemistry, resulting in relatively low removal efficiency for antibiotics. Generally, the biochar activated by chemical reagents was more efficient than physical methods [22]. Chemical activation can increase biochar's specific surface area and pore volume and effectively improve the oxygen-containing functional groups. Therefore, it is commonly used to modify biochar to enhance its adsorption performance [23]. Li et al. [24] reported that H_3PO_4-activated pinecone biochar for Zn^{2+} removal from wastewater and showed that the prepared carbon had excellent adsorption capacity (20 mg L^{-1}) and good regeneration performance. Taheran [25] improved the adsorption efficiency of biochar by NaOH treatment and reached the optimum adsorption capacity (208.3 mg g^{-1}) for chlortetracycline (CTC). Although using pinecone biochar for removing antibiotics, heavy metal ions, and dyes has already been reported, no study has been done on using pinecone carbon adsorbents for CAP removal from water.

In this study, pinecone-based biochar was prepared using KOH as a chemical activator at three different activation ratios. Batch experiments were conducted to examine the effects of initial pH, dosage, and reaction temperature on the CAP removal process. In addition, dynamic and isothermal modeling was employed to evaluate the CAP adsorption behavior onto the activated carbon. Finally, the interaction mechanism between KOH-activated biochar and CAP was elucidated through characterization and simulation results.

2 | Materials and Methods

2.1 | Chemicals

The raw biomass, pinecones, was easily collected from the seaside of Fukuoka City, Japan. After that, they were washed, dried, crushed, and sieved to obtain the precursor samples. HCl (1 mol L^{-1}), KOH, NaOH, and chloramphenicol (CAP) were purchased from Sigma Aldrich. The materials and chemicals are analytically pure and have not been further purified or modified.

2.2 | Synthesis of Pinecone Biochar

The biochar prepared in this work was obtained by chemical activation. Figure 1 describes the procedure in detail. In a typical synthesis, pinecones were subjected to pre-treatments to obtain precursor powders. The powder samples were pyrolyzed at 600°C for 1 h (heating rate: 5°C min^{-1}). The biochar was

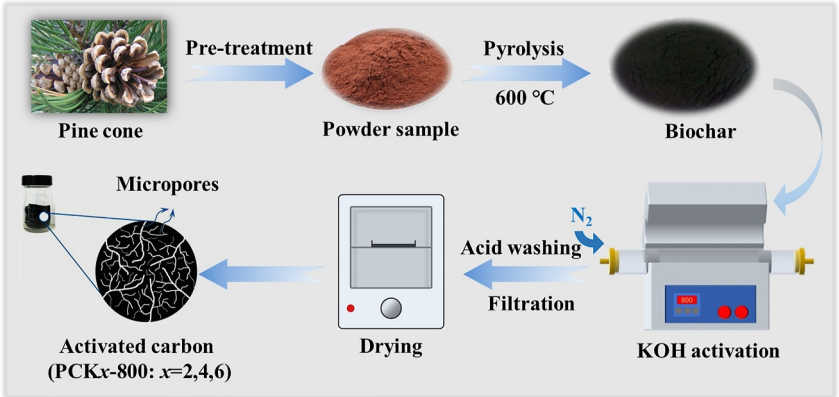

FIGURE 1 | The synthesis process of the PCKx-800 biochars from waste pinecone.

cooled and named PC600. To obtain the activated carbon, 1 g of biochar was thoroughly mixed with 2, 4, and 6 g of KOH solids, respectively. Subsequently, the above mixture was activated at 800°C for one hour in a N_2 atmosphere. After cooling, the biochar was ground and sieved (100 mesh).

Finally, the carbons were washed repeatedly with deionized water and 1 M HCl solution. The washing process involved soaking the carbon in the acid solution for 4 h with intermittent stirring 3 times, followed by repeated rinsing with deionized water until the pH stabilized at neutrality (approximately pH 7), indicating the complete removal of residual acid and impurities. It was then dried in a vacuum oven overnight at 80°C to remove moisture and other volatile materials. The final activated carbon samples were named PCK2-800, PCK4-800, PCK6-800.

2.3 | Characterization

The yield of the synthesized carbon was calculated by Equation (1) as follows:

$$\text{Yield (wt\%)} = \frac{\text{Mass of sample before treatment}}{\text{Mass of precursor material}} \times 100\% \quad (1)$$

N_2 adsorption/desorption isotherm was performed at 77K on the synthesized biochars to obtain the porous properties using a 3FLEX surface analyzer (Micromeritics Instruments, Japan). The samples were degassed under vacuum for 6 h before the measurement. A JSM-7900F scanning electron microscope (SEM) was employed to observe the microscopic morphology of the samples up to a magnification of 10,000. The functional groups were determined by an FT-IR spectrometer (Nicolet iN10). The activated carbon's zero charge (pH_{pzc}) was determined primarily using the salt addition method. 5 mg of PCK4-800 and 0.01 M NaCl solution (50 mL) were mixed and stirred at 25°C for one day. The initial pH was adjusted to 2.0–11.0 (using 0.1 mol L^{-1} HCl or NaOH), and the intersection of the curve with the *x*-axis obtained by recording the change in pH was considered to be the equipotential charge point of PCK4-800.

2.4 | Batch Experiments

Three hours of batch experiments were performed to evaluate the adsorption capacity of different activated carbon samples. The experiments were conducted with an initial concentration of 100 mg L^{-1} and a pH value of 6.32 for the CAP solution. One-way Analysis of Variance was used to control the dosage (0.05–0.3 g L^{-1}), initial pH (3–11), and reaction temperature (298–318 K) to investigate the different impact factors on the adsorption process.

In adsorption kinetics experiments, 5 mg biochar was added to a solution of 50 mL with 100 mg L^{-1} CAP amount at 298 K. After a specific time, the samples were collected until an adsorption equilibrium was reached. An adsorption isotherm was drawn according to the dependence of the adsorption capacity on the equilibrium concentration by changing the CAP initial concentration. The adsorption thermodynamics were examined at 298, 308, and 318 K. The experimental data were fitted using several kinetic and isothermal models.

The solution was taken 2 mL at a time and filtered using a membrane filter (0.45 μm). Then, they were further analyzed using a UV-VIS spectrophotometer. The adsorption capacity and removal rate were calculated through Equations (2) and (3) to evaluate the performance of different activated carbon adsorbents for CAP removal from aqueous environments.

$$q_t = \frac{V(C_0 - C_t)}{m} \quad (2)$$

$$R\,(\%) = \frac{C_0 - C_t}{C_0} \times 100 \quad (3)$$

2.5 | Adsorption Kinetic

In the kinetic experiment, 5 mg of biochar was added to the CAP solution of 50 mL at various initial concentrations (50, 100, 200 mg L^{-1}) and shaken at 298 K and 1000 rpm for 180 min. A certain amount of adsorbent was collected at different intervals (5, 10, 15, 20, 25, 30, 40, 50, 60, 90, 120, 150, and 180 min) and tested the residual concentration of CAP. The pseudo-first-order (PFO) and pseudo-second-order (PSO) kinetic models were applied to fit the experimental data, which can evaluate the adsorption mechanism between CAP molecules and the modified biochar. The formulas are shown in Equations (4) and (5).

$$\ln(q_e - q_t) = \ln q_e - k_1 t \quad (4)$$

$$\frac{t}{q_t} = \frac{1}{k_2 {q_e}^2} + \frac{t}{q_e} \quad (5)$$

2.6 | Adsorption Isotherm

The adsorption experiments were conducted at various initial concentrations (30, 50, 80, 100, 150, 200, and 300 mg L^{-1}) and different temperatures (298, 308, and 318 K). After equilibration, the remaining CAP solution concentration was determined. The Langmuir and Freundlich isotherm models were used to fit the obtained experimental data, and the relevant parameters were estimated and analyzed by non-linear regression to determine the adsorption characteristics. The calculation equations are represented in Equations (6) and (7).

$$q_e = \frac{K_L q_m C_e}{1 + K_L C_e} \quad (6)$$

$$q_e = K_F {C_e}^{1/n} \quad (7)$$

2.7 | Adsorption Thermodynamic

The main objective of the thermodynamic analysis was to elucidate the primary mechanism of antibiotic removal by activated

carbon. The relevant thermodynamic parameters (Equations (8)–(11)) were estimated using the Van't Hoff equation.

$$K_D = \frac{q_e}{C_e} \tag{8}$$

$$\Delta G^0 = -RT \ln K_D \tag{9}$$

$$\Delta G^0 = \Delta H^0 - T\Delta S^0 \tag{10}$$

$$\ln K_D = \frac{\Delta S^0}{R} - \frac{\Delta H^0}{RT} \tag{11}$$

2.8 | Regeneration Property

The regenerability of the activated carbon was evaluated by multiple adsorption-desorption cycle experiments. The CAP was desorbed with a mixture of ethanol and 0.1 mol L^{-1} HCl (volume ratio 1:1, pH = 1). The used PCK4-800 was first vacuum filtered and ultrasonicated in the emulsion solution at 45°C for 30 min, followed by stirring for 24 h. The activated carbon was then collected by vacuum filtration, rinsed with deionized water and ethanol, and finally placed in a drying oven at 100°C overnight. The residual concentration of CAP was determined when the adsorption process ended, and the removal rate and adsorption capacity were calculated.

3 | Results and Discussion

3.1 | Characterization of Pinecone Biochar

3.1.1 | SEM

The microstructure of PC600 and PCK*x*-800 was characterized by SEM (Figure 2). It was seen that there is a significant difference between their morphology and pore structure. Compared to the smooth and dense surface of PC600, a clear pore structure was observed on the surface of the KOH-activated biochar. At high temperatures, K^+ and OH^- produced by the decomposition of KOH were reacted with carbon atoms. The generated products (K_2CO_3 and K_2O) caused corrosion and reorganization of the carbon skeleton, which increased the biochar's specific surface area and pore size [26]. The potassium metal generated from the carbon-reduced potassium compounds effectively inserts into the carbon matrix, leading to lattice expansion and promoting further expansion of the pore structure [27]. Therefore, PCK*x*-800 (Figure 2b-d) has a rough surface and a graded porous structure. In addition, with increased KOH ratio, the surface particles were almost completely disintegrated, and the pore size increased. For PCK6-800 (Figure 2d), the carbon skeleton structure collapsed, and the grooves on the surface were destroyed due to the excessive amount of activator. This phenomenon illustrates that the degree of activation greatly influences the pore structure of bio-

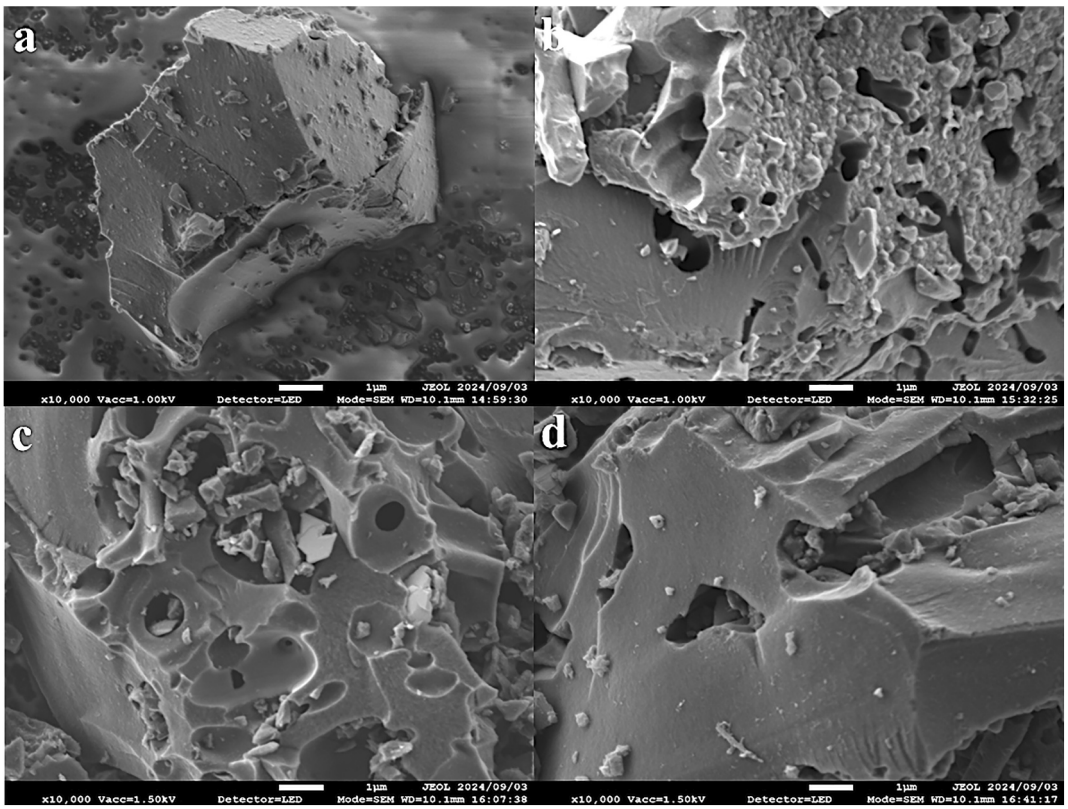

FIGURE 2 | The SEM images of carbonized and activated pinecone: (a) PC600; (b) PCK2-800; (c) PCK4-800; (d) PCK6-800.

char, which is directly related to the activator dosage and activation time.

3.1.2 | FT-IR

The FT-IR spectra of different biochars are shown in Figure 3a. All samples had a broader weak peak near 3500 cm^{-1}, attributed to the stretching vibration of -OH. This peak gradually weakened as the activation ratio increased, indicating a more complete activation. The multiple peaks in the 1000–1500 cm^{-1} region may be related to the vibration of C-O or C-H bonds. It noted that certain oxidizing functional groups were introduced during the activation treatment. The peaks in 1500–1700 cm^{-1} are associated with the vibration of C=C, suggesting that more graphitized carbon may be present in the char structure with increasing activation [28]. As the ratio of KOH increased, the characteristic absorption peaks appeared in the low-wave number region (1000–1500 cm^{-1}) gradually enhanced, indicating that more oxidized groups and defective structures were introduced. KOH activation effectively improved the oxygen-containing functional groups on the carbon material surfaces, which was conducive to improving their adsorption properties.

The FT-IR of PCK4-800 before and after the adsorption of CAP was also examined as shown in Figure 3b. Compared to pristine PCK4-800, PCK4-800 (CAP) showed new absorption peaks around 1500–1750 cm^{-1}, which corresponded to the stretching vibrations of the C=O bond and were related to the amide and carboxylic acid functional groups of CAP. It indicated the CAP molecule was bound to PCK4-800 through specific forces. The appearance of new absorption peaks near 3500–3900 cm^{-1} indicated that the O-H or N-H groups of CAP still appeared, confirming that chloramphenicol was successfully adsorbed. Therefore, the adsorption process primarily depends on the interaction of the surface of activated carbon with the hydroxyl, amino, or carbonyl groups of chloramphenicol.

3.1.3 | BET

Figure 4a,b show the N_2 adsorption/desorption isotherms and pore size distribution, respectively. According to IUPAC's definition of adsorption isotherms, PC600 and PCK2-800 belong to type I. PCK4-800 and PCK6-800 showed adsorption behaviors between type I and type IV, with H_4 hysteresis loops at relative pressure $P/P_0 > 4.5$ [29]. It indicated the combined contribution of micropores and mesopores in the porous structure of the

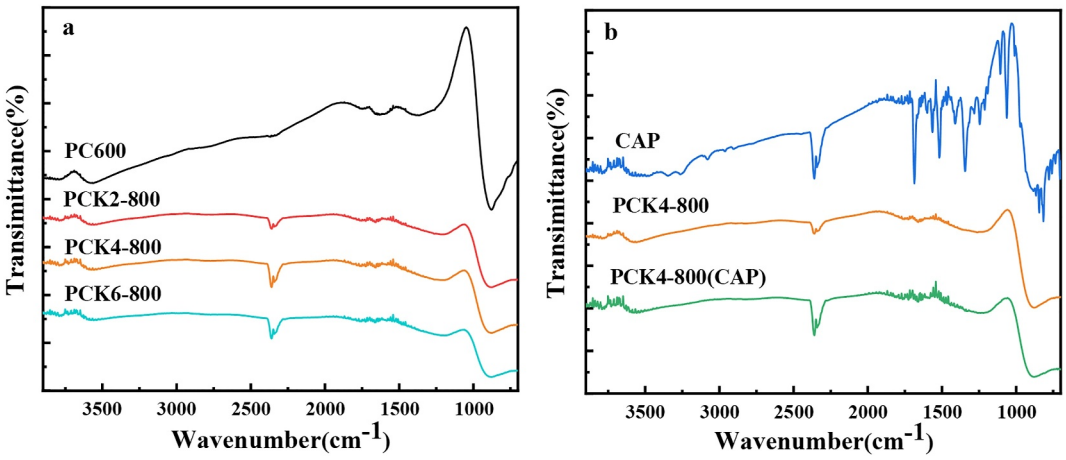

FIGURE 3 | FT-IR spectra of (a) synthesized biochars at different activation conditions, (b) PCK4-800 before and after CAP removal in water.

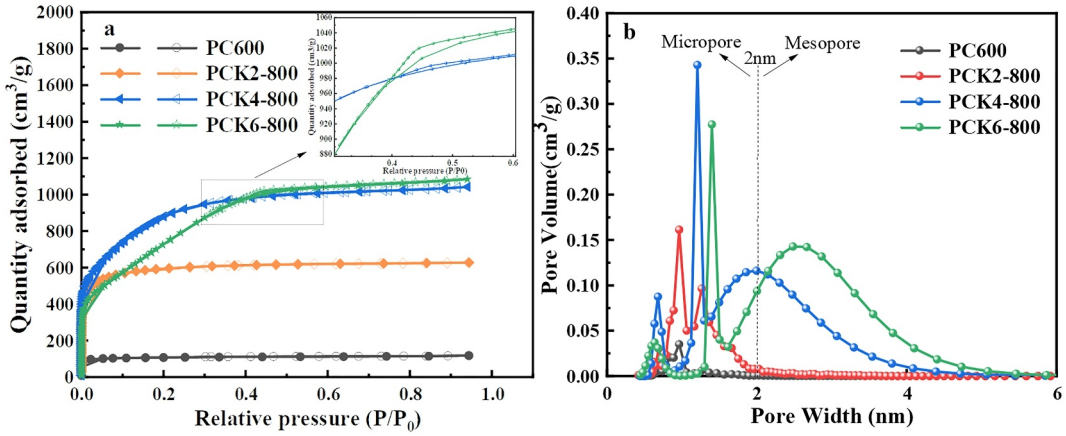

FIGURE 4 | (a) N_2 adsorption and desorption isotherm and (b) pore size distribution.

adsorbents. Figure 4b also confirmed the presence of mesopores, which facilitated the adsorption of antibiotic macromolecular pollutants, illustrating that the prepared KOH-activated biochar was a micro mesoporous material.

Table 1 summarizes the calculated SSA, total pore volume, and activation yield. The SSA of PCK4-800 at an activation ratio of 4:1 was significantly increased to 3131.60 $m^2\ g^{-1}$, which was much higher than PC600 (595.05 $m^2\ g^{-1}$) and PCK2-800 (2493.86 $m^2\ g^{-1}$). Such an increase results from a uniform pore structure produced by internal etching. The decrease in SSA of PCK6-800 may be related to pore collapse and corrosion caused by over-activation, which is consistent with the SEM results [30]. Other studies have reported similar results [31]. Moreover, the pore volume increased to 1.848 $cm^3\ g^{-1}$ with the rise of the activation ratio, while the activation yield became lower and lower, indicating a more thorough activation. The results showed that the activation ratio greatly influences the pore structure of activated carbon. With the well-developed pore structure of the prepared KOH-activated biochar, it is likely that CAP molecules will be effectively attracted to the biochar's surface and internal pores via pore filling [32].

3.2 | Impact Factors for CAP Removal

3.2.1 | Effect of KOH Ratio

Most studies have shown that increasing the ratio of KOH to the material will improve the SSA and increase the adsorption capacity of antibiotics. Figure 5a demonstrates the effect of the KOH ratio increase on antibiotic removal from biochar. Overall, the adsorption of antibiotics on the four biochars was accompanied by two phases: a rapid increase of removal within the initial 30 min and a stabilization process during 30–180 min. During the initial rapid adsorption stage, abundant adsorption sites of the biochar surface were available, and CAP was rapidly adsorbed onto these active sites. After that, a higher concentration gradient increased the mass transfer rate from the

TABLE 1 | Physicochemical properties of the synthesized activated carbons.

Sample	Activation ratio	Specific surface area S_{BET} ($m^2\ g^{-1}$)	Total pore volume v_p ($cm^3\ g^{-1}$)	Activation yield (%)
PC600	/	595.05	0.170	/
PCK2-800	2:1	2493.86	0.887	55.7
PCK4-800	4:1	3131.60	1.800	52.7
PCK6-800	6:1	2768.60	1.848	50.3

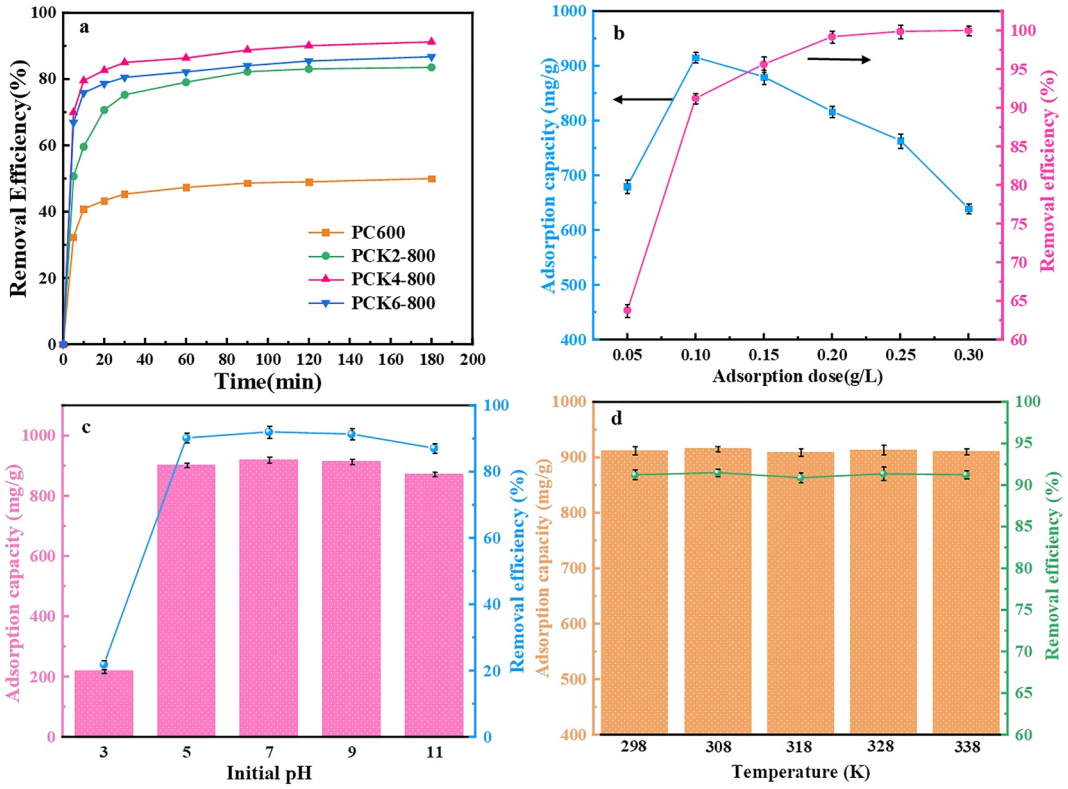

FIGURE 5 | The impact factors of CAP removal on pinecone biochar: (a) Effect of contact time; (b) Effect of adsorbent dosage; (c) Effect of initial pH; (d) Effect of temperature.

solution to the adsorbent surface [33]. Most adsorption sites were saturated with CAP molecules during the stabilization period, leading to a stable removal rate. It indicates that the adsorption can reach equilibrium at 180 min. It can be observed that the increased activation ratio improved the CAP removal rate. In particular, the removal rate of PCK4-800 reached 85% after 30 min and 91% at equilibrium, which is 1.8 times higher than the removal efficiency of PC600 (50%). From the economic and adsorption performance viewpoints, PCK4-800 was selected as the best adsorbent to be further explored in subsequent experiments.

3.2.2 | Effect of Adsorbent Dosage

The effect of adsorbent dosage on CAP removal by PCK4-800 is shown in Figure 5b. As the dosage increased to 0.3 g L^{-1}, the removal efficiency increased largely to 100%. The increase in adsorbent dose promotes the interaction between CAP molecules and more adsorption sites, contributing to the adsorption capacity. However, the sorption capacity showed an increasing and then decreasing trend due to the increased diffusion path of the adsorbent and the overlapping adsorption sites, and reached a maximum value (915.74 mg g^{-1}) at the adsorbent dosage of 0.1 g L^{-1} [34]. Therefore, from an economic and adsorption effect viewpoint, the optimum adsorbent dosage was 0.1 g L^{-1}, and the removal efficiency could reach 91.22% under this condition.

3.2.3 | Effect of Initial pH

The initial pH can affect the surface charge characteristics of the biochar and the morphology of antibiotics. Figure 6 characterizes the charge distribution on the biochar surface. The pH_{PZC} of PCK4-800 is 5.94, at which point the sample is neutral. When the pH is lower than 5.94, PCK4-800 is negatively charged, and when greater than 5.94, it is positively charged. Besides, researchers reported that CAP has a pKa of 5.5, and when the pH is higher than 5.5, chloramphenicol deprotonates to become CAP^{-}. Figure 5c shows how the initial pH affected the CAP removal process. At pH 3.0, the CAP removal efficiency decreased sharply to only 21.8% compared with the natural pH (pH_0 = 6.32). However, as the pH increased to 7.0, the CAP removal rate rapidly increased to a maximum of 92.0%. Interestingly, the adsorption performance of PCK4-800 for CAP adsorption did not change remarkably when the pH rose to 11.0. A higher CAP removal rate was observed for pH values between 6.0 and 11.0, suggesting that the surface of the biochar plays a positive role in terms of positive charge. Under this condition, the adsorbent and the pollutant were bound together mainly through electrostatic interactions and hydrogen bonding, significantly improving the removal effect. The removal rate between 5.0 and 6.0 was still high over 90%, which suggested that except for electrostatic interactions, π-π interactions or hydrogen bonding might also exist. Therefore, the biochar PCK4-800 synthesized in this study can adapt to a wide pH range of acidity and alkalinity, and has a broad practical application value. In the subsequent study, an excellent adsorption effect can be achieved without pre-adjusting the pH of the CAP.

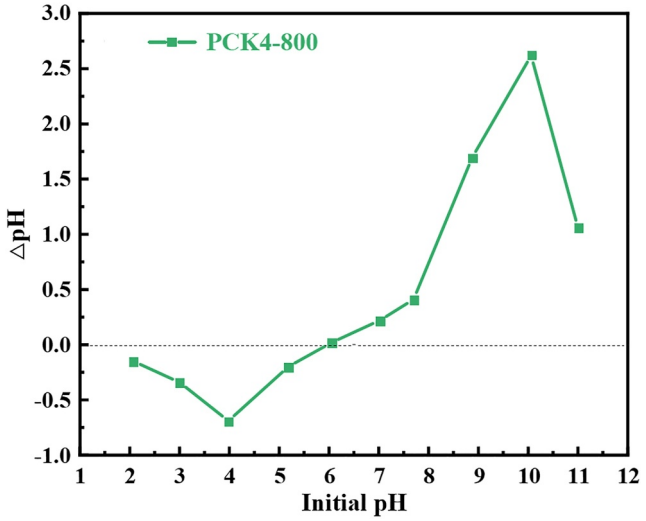

FIGURE 6 | The zero electric charge (pH_{pzc}) of PCK4-800.

3.2.4 | Effect of Reactive Temperature

Figure 5d described the reaction temperature effect on the CAP adsorption onto PCK4-800. Three hours were taken as the adsorption equilibrium time, and the removal rate was recorded at more than 90% at all temperatures. The PCK4-800 adsorption capacity increased slightly with increasing reaction temperature, indicating that the sorption was endothermic [35]. However, there was no significant increase in the removal rate due to higher reaction temperatures, concordantly with the findings of Idham et al. [36]. Consequently, the reaction temperature has little influence on the adsorption process, demonstrating that the CAP adsorption by PCK4-800 is mainly dominated by chemical adsorption. Considering the practical application and economy, the reaction temperature was chosen to be 298 K (the adsorption capacity was 912.2 mg g^{-1}).

3.3 | Adsorption Kinetic Analysis

It is beneficial in emphasizing the speed-limiting step and revealing the adsorption mechanism by adsorption kinetics. To characterize the adsorption process, we selected three initial concentrations of CAP and measured the adsorption volume at different times. Figure 7 displayed the adsorption kinetic profiles of CAP on PCK4-800 at three different initial concentrations. Overall, the rapid adsorption occurred in the initial 30 min because abundant adsorption sites were available for CAP binding in the early stage of the reaction. The adsorption gradually reached equilibrium in the second stage within 30–180 min. It was easily found that the CAP adsorption capacity (from 400 to 1400 mg g^{-1}) is proportional to the initial concentration. Probably because the concentration difference provided a larger driving force, the adsorption sites on the biochar surface were taken by more adsorbate [37]. In addition, the higher concentration of solute molecules enhanced interaction with the biochar surface, which in turn increased the adsorption capacity.

Table 2 shows several parameters of the PFO and PSO kinetic models fitted to the experimental data. By comparing the R^2 (correlation coefficients), the R^2 of the PSO model were all more than 0.99900, which was higher than the PFO model (0.98984–0.99296). The results indicated that the PSO model described the adsorption process better, implying a predominance of the adsorption process by chemical adsorption. In addition, there is a closer approximation to the experimental data for the adsorption capacity calculated from the PSO model.

3.4 | Adsorption Isotherm Analysis

Langmuir and Freundlich models simulated adsorption data at various temperatures, which are shown in Figure 8. Table 3 furnishes the relevant fitting data. Compared to the Freundlich model, the R^2 of the Langmuir model is closer to 1 ($R^2 > 0.98$), indicating that monolayer adsorption is the primary mechanism. The maximum monolayer adsorption capacity (q_{max}) of PCK4-800 was 1991.19 mg g^{-1} at 298 K. The significant SSA and abundant oxygen-containing functional groups greatly enhance the removal efficiency, which is competitive with recently reported adsorbents (Table 4). It shows that PCK4-800 is a low-cost and efficient adsorbent.

3.5 | Adsorption Thermodynamic Analysis

The thermodynamic data in Table 5 provide insights into the removal process of chloramphenicol on activated carbon. Table 5 listed the calculated thermodynamic parameters at different temperatures. The negative ΔG^0 proved the thermodynamic feasibility and spontaneous proceeding for CAP onto the activated carbon. And ΔG^0 decreased with increasing

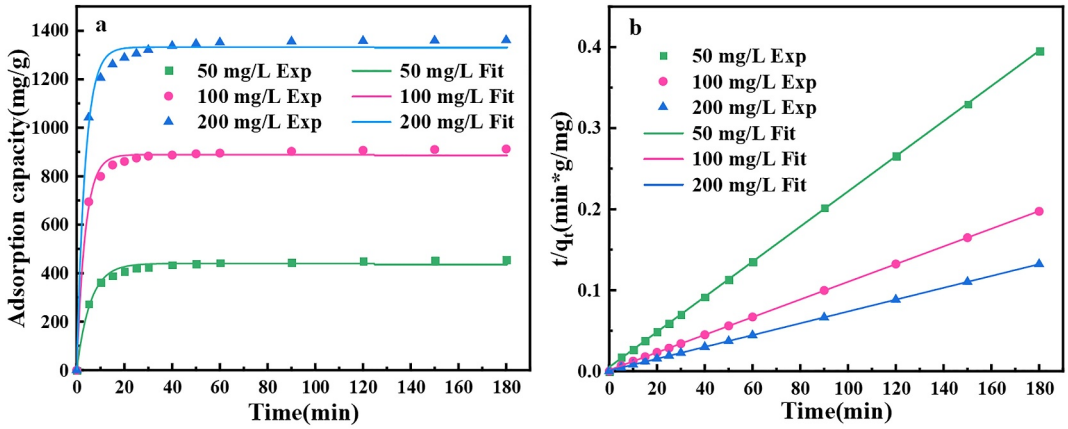

FIGURE 7 | The kinetic models were fitted to the experimental data. (a) Pseudo-first-order (PFO); (b) Pseudo-second-order (PSO).

TABLE 2 | Fitting values of the adsorption kinetic models for CAP by 0.1 g L^{-1} PCK4-800.

CAP initial concentration (mg L^{-1})	Pseudo-first-order			Pseudo-second-order		
	q_e (mg g^{-1})	k_1 (min^{-1})	R^2	q_e (mg g^{-1})	k_2 (g (mg min) $^{-1}$)	R^2
50	440.04	0.175	0.98984	460.83	0.000913	0.99981
100	888.74	0.280	0.99312	943.40	0.000845	0.99995
200	1332.21	0.282	0.99296	1369.88	0.000685	0.99996

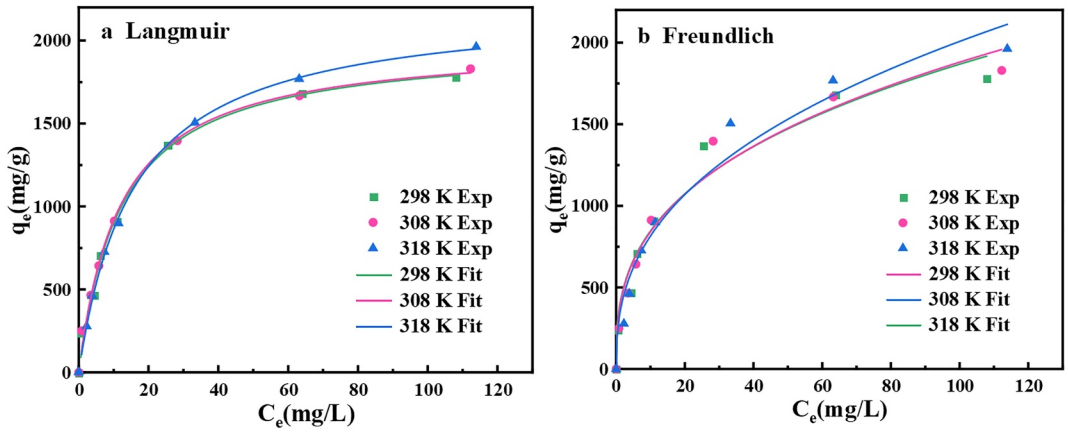

FIGURE 8 | Adsorption isotherms simulated with (a) Langmuir and (b) Freundlich models.

TABLE 3 | Adsorption isotherm data was obtained using Langmuir and Freundlich models.

	Langmuir			Freundlich		
Temperature (K)	q_m (mg g^{-1})	K_L (L mg^{-1})	R^2	K_F (L mg^{-1})	n	R^2
298	1991.19	0.0826	0.98593	383.44	2.909	0.96664
308	1994.50	0.0851	0.99246	376.44	2.863	0.97329
318	2218.50	0.0638	0.99906	331.25	2.556	0.96887

TABLE 4 | CAP adsorption performance of various adsorbents.

Adsorbent	pH	C_0 (mg L^{-1})	Tem. (°C)	Dosage (g L^{-1})	q_m (mg g^{-1})	Ref.
Peanut shell-based biochar	7	300	40	1	423.7	[38]
Enteromorpha prolifera -based activated carbon	—	400–1000	20	0.5	709.2	[39]
Core-shell surface imprinted polymers based on magnetic chitosan	—	32.31	25	0.5	403.92	[40]
Nanoscale zero-valent iron-supported biochar	7	150	50	0.02	1563.97	[41]
Hierarchical porous biochar from sodium carboxymethyl cellulose	3	150	45	0.2	879.68	[42]
Shrimp shell-based hierarchical porous carbons	6.94	200	45	0.3	742.4	[43]
Pinecone-based activated carbon	6.32	100	25	0.1	1991.19	Present study

TABLE 5 | Thermodynamic data for CAP removal.

Temperature (K)	$\ln K_D$	ΔG^0 (kJ mol^{-1})	ΔH^0 (kJ mol^{-1})	ΔS^0 (J $(mol\ K)^{-1}$)	R^2
298	4.371	−10.94	4.68	52.04	0.996
308	4.426	−11.51			
318	4.490	−11.56			

temperature, indicating that higher temperature provides a more significant driving force. In addition, positive values of ΔH^0 indicated the adsorption process was endothermic. The entropy change value ΔS^0 was positive, suggesting that the randomness and disorder at the solid-liquid interface between the adsorbent and the adsorbate increased.

3.6 | Effect of Coexisting Ions

Industrial and medical wastewater typically contains a variety of anions and cations, and these co-existing ions may affect the adsorption performance of the activated carbon through mechanisms such as competitive adsorption, charge neutralization, or alteration of the chemical environment in solution. Therefore, it is important to fully investigate the effect of coexisting ions on CAP removal by PCK4-800 in order to optimize the adsorption conditions. It also provides some theoretical foundations for the practical application of activated carbon in complex environments. Figure 9 explored the effect of three cations (Na^+, Ca^{2+}, Mg^{2+}) and three anions (NO_3^-, $H_2PO_4^-$, Cl^-).

Figure 9a showed that Na^+ slightly reduced the removal of CAP with a reduction of 3.97%. On the contrary, the divalent cations Ca^{2+} and Mg^{2+} had stronger inhibitory effects than Na^+, and the CAP removal efficiency decreased by 9.55% and 5.98% when the concentration was increased from 0 to 20 mM. The negative effects of cations on CAP removal by PCK4-800 were in the order of $Na^+ < Mg^{2+} < Ca^{2+}$. Divalent cations have a higher charge density and are more likely to interact electrostatically with negatively charged functional groups (e.g., carboxyl and hydroxyl) on the biochar surface than monovalent ions, which occupy the adsorption sites and thus reduce the adsorption of CAP [44, 45].

Figure 9b depicted that monovalent Cl^- hardly affected the adsorption effect of CAP as the removal efficiency decreased from 90.2% to 89.1%. Secondly, the removal efficiency decreased to 86% when the concentration of $H_2PO_4^-$ ion was increased from 0 to 20 mM. While NO_3^- showed a strong inhibitory effect. The overall order of negative effects was $Cl^- < H_2PO_4^- < NO_3^-$. Cl^- responded weakly to surface repulsion due to its lower hydration energy and polarity. $H_2PO_4^-$ was detected on the activated carbon surface through the interaction with functional groups by hydrogen bond formation, which increased the adsorption tendency. On the other hand, it has been well proved in the literature that NO_3^- significantly reduces the adsorption capacity of chloramphenicol by altering the polarity of the solution and the adsorption site charge distribution [46].

3.7 | Regeneration Property of Adsorbent

Overall, the recyclability of biochar is more economical in practical applications. Figure 10 examined the removal efficiency after five cycles using the mixture solution to desorb CAP from the biochar. The removal rate of biochar gradually decreased with increasing desorption cycles, attributed to the

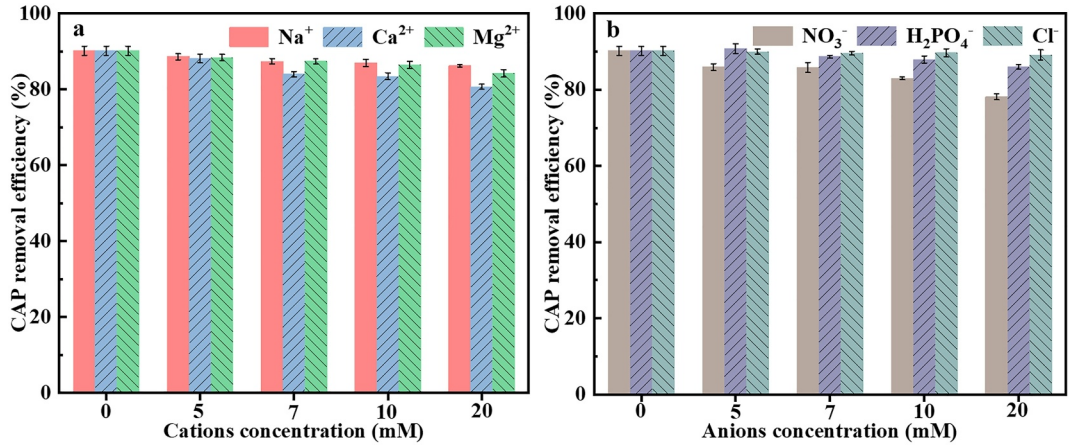

FIGURE 9 | Effect of coexisting ions on the performance of PCK4-800. (a) Cations, (b) Anions.

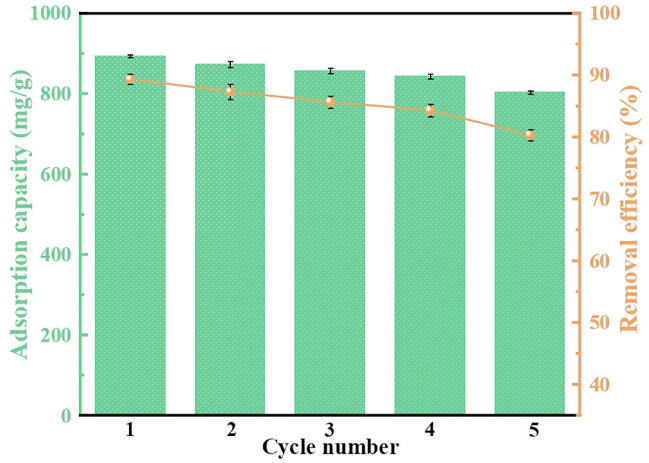

FIGURE 10 | The stability and recyclability of PCK4-800 on CAP adsorption.

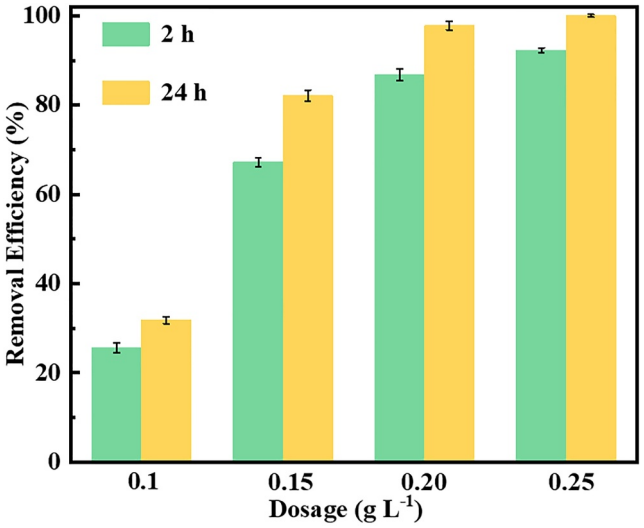

FIGURE 11 | The performance of PCK4-800 in removing CAP from river water at different time intervals and dosages.

CAP occupying the available active sites of biochar. However, the adsorption performance of PCK4-800 remained excellent after four cycles, with the removal rate and adsorption capacity of 84.3% and 843.3 mg g^{-1}, respectively. After five elutions, CAP removal was maintained above 80.35%, with a 10.9% reduction in adsorption capacity. It confirmed the superior regenerability of PCK4-800 after five cycles of regeneration, so the pinecone-based activated carbon is an efficient and economic antibiotic adsorbent.

3.8 | Practical Applicability

To examine the practical application potential of PCK4-800, the batch adsorption experiments were conducted by collecting natural surface water from rivers in Fukuoka City, Japan. Figure 11 demonstrates the true CAP (20 mg L^{-1}) removal efficiency of PCK4-800 at different time intervals and dosages. At the low dose of 0.1 g L^{-1}, the adsorbent didn't seem to have favorable results. As the dosage was increased to 0.15 g L^{-1}, the adsorption effect was significantly enhanced, and more than 80% CAP removal efficiency could be achieved within 24 h. More interestingly, when the dosage was further increased to 0.2 g L^{-1}, it was feasible to remove almost 100% of CAP from natural surface water within 24 h. At low doses, the removal efficiency of CAP is low due to the limited amount of active adsorption sites on the biochar surface. It is particularly obvious in complex aqueous environments. Therefore, increasing the dose can provide more adsorption sites and thus enhance the removal effect of CAP. The results of this experiment verified this trend. It proves the feasibility of using PCK4-800 to remove CAP in real aqueous environments.

3.9 | Adsorption Mechanisms

Through characterization of the chemical adsorption structure of the biochar, batch experiments, and model fitting analysis, the mechanism of CAP adsorption on PCK4-800 is hypothesized, as shown in Figure 12. BET and SEM results proved that the surface of PCK4-800 became roughened and exhibited extremely high SSA, which could provide more adsorption active sites for CAP. Moreover, the adsorption capacity was positively correlated with the SSA of the biochar, indicating that the pore filling was the primary adsorption mechanism [47]. The adsorption kinetics analysis revealed that chemical adsorption played a significant

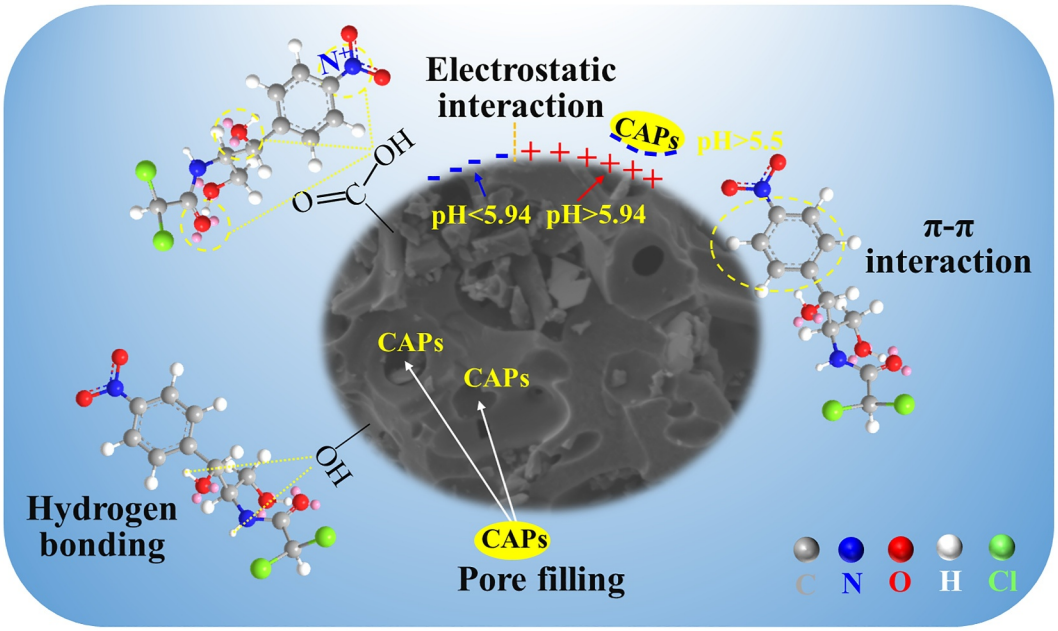

FIGURE 12 | The adsorption mechanisms of CAP onto the biochars.

role and was governed by the pore-filling mechanism as a consequence of oxygenated functional groups. The FTIR results indicated that there are C=C functional groups and a π-electron-rich graphitized structure on the biochar surface; it can serve as a π-electron donor. Meanwhile, CAP has an aromatic ring and a strong electron-absorbing group $-NO_2$ [48]. Therefore, the adsorption of CAP on PCK4-800 can be realized by a π-π donor-acceptor mechanism. In addition, it was confirmed that electrostatic interaction was also a crucial mechanism since pH strongly affected removal efficiency. The pH_{pzc} of PCK4-800 was 5.94, and the biochar surface was positively charged when pH > 5.94. When the pH was higher than 5.94, the CAP was negatively charged and electrostatically interacted with the positively charged biochar, which enhanced the adsorption of chloramphenicol. At pH = 5, the CAP removal rate was still as high as 90%, indicating that except for electrostatic interactions, both π-π interaction and hydrogen bonding mechanisms also contributed to the adsorption process.

In conclusion, the CAP adsorption onto PCK4-800 is governed by a combination of the primary mechanism of pore filling and π-π interactions and a secondary mechanism such as electrostatic effects and hydrogen bonding. In fact, the adsorption of antibiotics by biochar is not a homogenous action; the collaborative effect of these mechanisms provides this biochar with excellent adsorption potential.

4 | Conclusions

In this study, high specific surface area pinecone-based biochar was successfully prepared using KOH activation, and batch experiments demonstrated its excellent potential for removing chloramphenicol (CAP) from aqueous environments. The KOH-activated biochar exhibited a highly developed surface area and pore volume (3131.60 $m^2\ g^{-1}$ and 1.80 $cm^3\ g^{-1}$, respectively), and the FTIR results confirmed the presence of abundant oxygen-containing functional groups on its surface. Batch experiments further revealed that PCK4-800 achieved the highest CAP removal efficiency and adsorption capacity (91.22% and 912.2 mg g^{-1}), with a positive correlation between adsorption capacity and the specific surface area. The adsorption process followed the pseudo-second-order kinetic model and Langmuir isotherm, indicating monolayer and chemical adsorption. The calorimetric values confirmed that the process was spontaneous and endothermic. After three desorption cycles using hydrochloric acid with ethanol, the biochar retained a removal rate of 80%. The dominant mechanisms for CAP adsorption included electrostatic interactions, pore filling, hydrogen bonding, and π-π interactions.

The results showed that biochar made from pinecone with a high specific surface area is an efficient and cost-effective adsorbent with promising potential for antibiotic removal. In addition, PCK4-800 is stable enough to work under a wide pH range (5–11) and temperature range (298–338 K) and can be recycled for economic effect. In summary, this study is expected to provide possible value for future large-scale wastewater treatment technologies.

Acknowledgments

This work was supported by a scholarship from China Scholarship Council (No. 202307040018).

Conflicts of Interest

The authors declare no conflicts of interest.

Data Availability Statement

Data will be available on request.

References

1. O. Falyouna, I. Maamoun, K. Bensaida, A. Tahara, Y. Sugihara, and O. Eljamal, "Encapsulation of Iron Nanoparticles With Magnesium Hydroxide Shell for Remarkable Removal of Ciprofloxacin From Contaminated Water," *Journal of Colloid and Interface Science* 605 (2022): 813–827, https://doi.org/10.1016/j.jcis.2021.07.154.

2. F. Saremi, M. R. Miroliaei, N. M. Shahabi, and H. Sheibani, "Adsorption of Tetracycline Antibiotic from Aqueous Solutions onto Vitamin B6-upgraded Biochar Derived From Date Palm Leaves,"*Journal of Molecular Liquids* 318 (2020): 114126. https://doi.org/10.1016/j.molliq.2020.114126.

3. B. L. Phoon, C. C. Ong, M. S. M. Saheed, et al. "Conventional and Emerging Technologies for Removal of Antibiotics From Wastewater," *Journal of Hazardous Materials* 400 (2020): 12296. https://doi.org/10.1016/j.jhazmat.2020.122961.

4. X. Wang, R. Yin, L. Zeng, and M. Zhu, "A Review of Graphene-Based Nanomaterials for Removal of Antibiotics From Aqueous Environments," *Environment and Pollution* 253 (2019): 100–110, https://doi.org/10.1016/j.envpol.2019.06.067.

5. X. Liu, Z. Cao, Z. L. Yuan, et al., "Insight into the Kinetics and Mechanism of Removal of Aqueous Chlorinated Nitroaromatic Antibiotic Chloramphenicol by Nanoscale Zero-Valent Iron," *Chemical Engineering Journal* 334 (2018): 508–518, https://doi.org/10.1016/j.cej.2017.10.060.

6. Y. Cao, W. Qiu, Y. M. Zhao, et al., "The Degradation of Chloramphenicol by O3/PMS and the Impact of O3-Based AOPs Pre-Oxidation on Dichloroacetamide Generation in Post-Chlorination," *Chemical Engineering Journal* 401 (2020): 126146, https://doi.org/10.1016/j.cej.2020.126146.

7. N. A. Ahammad, M. A. Zulkifli, M. A. Ahmad, B. H. Hameed, and A. T. Mohd Din, "Desorption of Chloramphenicol From Ordered Mesoporous Carbon-Alginate Beads: Effects of Operating Parameters, and Isotherm, Kinetics, and Regeneration Studies," *Journal of Environmental Chemical Engineering* 9, no. 1 (2021): 105015, https://doi.org/10.1016/j.jece.2020.105015.

8. C. Li, F. Luo, H. J. Duan, et al., "Degradation of Chloramphenicol by Chlorine and Chlorine Dioxide in a Pilot-Scale Water Distribution System," *Separation and Purification Technology* 211 (2019): 564–570, https://doi.org/10.1016/j.seppur.2018.10.019.

9. A. Murata, H. Takada, K. Mutoh, H. Hosoda, A. Harada, and N. Nakada, "Nationwide Monitoring of Selected Antibiotics: Distribution and Sources of Sulfonamides, Trimethoprim, and Macrolides in Japanese Rivers," *Science of the Total Environment* 409, no. 24 (2011): 5305–5312, https://doi.org/10.1016/j.scitotenv.2011.09.014.

10. Z. X. Zhang, H. Y. Zhang, D. H. Tian, et al., "Luminescent Sensors for Residual Antibiotics Detection in Food: Recent Advances and Perspectives," *Coordination Chemistry Reviews* 498 (2024): 215455, https://doi.org/10.1016/j.ccr.2023.215455.

11. M. F. Idham, O. Falyouna, R. Eljamal, I. Maamoun, and O. Eljamal, "Chloramphenicol Removal From Water by Various Precursors to Enhance Graphene Oxide–iron Nanocomposites," *Journal of Water Process Engineering* 50 (2022): 1032289. https://doi.org/10.1016/j.jwpe.2022.103289.

12. C. J. Zhou, Y. J. Wang, L. Du, H. B. Yao, "Preparation of Highly Dispersed SiO2 Nanoparticles Using Continuous Gasbased Impinging Streams," *Chemical Engineering Journal* 327 (2017): 734–742, https://doi.org/10.1016/j.cej.2017.06.133.

13. G. DdH. C. Ll BaoWangQu, D. D. Bao, D. Q. Zhang, C. Wang, L. L. Qu, and H. T. Li, "Removal of Antibiotics From Water With an All-Carbon 3D Nanofiltration Membrane," *Nanoscale Research Letters* 13, no. 1 (2018): 146, https://doi.org/10.1186/s11671-018-2555-9.

14. O. Baaloudj, I. Assadi, N. Nasrallah, A. E. Jery, L. Khezami, and A. A. Assadi, "Simultaneous Removal of Antibiotics and Inactivation of Antibiotic-Resistant Bacteria by Photocatalysis: A Review," *Journal of Water Process Engineering* 42 (2021): 102089, https://doi.org/10.1016/j.jwpe.2021.102089.

15. P. J. M. Reis, A. C. Reis, B. Ricken, et al., "Biodegradation of Sulfamethoxazole and Other Sulfonamides by Achromobacter Denitrificans PR1," *Journal of Hazardous Materials* 280 (2014): 741–749, https://doi.org/10.1016/j.jhazmat.2014.08.039.

16. T. Ahmad, M. Saood, J. Georgin, et al. "Development of A New Hyper Crosslinked Resin Based on Polyamine-isocyanurate for the Efficient Removal of Endocrine Disruptor Bisphenol-A from Water," *Journal of Water Process Engineering* 53 (2023): 103623. https://doi.org/10.1016/j.jwpe.2023.103623.

17. M. A. Islam, S. H. Yoon, J. Miyawaki, and B. B. Saha, "Activated Carbon Derived From Waste Mangrove Biomass for Designing Heat Pumps With Improved Specific Cooling Capacity and Lower CO2 Emission," *International Communications in Heat and Mass Transfer* 158 (2024): 107828, https://doi.org/10.1016/j.icheatmasstransfer.2024.107828.

18. H. Sun, W. He, C. Zong, and L. Lu, "Template-Free Synthesis of Renewable Macroporous Carbon via Yeast Cells for High-Performance Supercapacitor Electrode Materials," *ACS Applied Materials & Interfaces* 5, no. 6 (2013): 2261–2268, https://doi.org/10.1021/am400206r.

19. S. Wang, J. H. Kwak, M. S. Islam, M. A. Naeth, M. Gamal El-Din, and S. X. Chang, "Biochar Surface Complexation and Ni(II), Cu(II), and Cd(II) Adsorption in Aqueous Solutions Depend on Feedstock Type," *Science of the Total Environment* 712 (2020): 136538, https://doi.org/10.1016/j.scitotenv.2020.136538.

20. M. S. Islam, J. H. Kwak, C. Nzediegwu, et al., "Biochar Heavy Metal Removal in Aqueous Solution Depends on Feedstock Type and Pyrolysis Purging Gas," *Environment and Pollution* 281 (2021): 117094, https://doi.org/10.1016/j.envpol.2021.117094.

21. G. Duman, Y. Onal, C. Okutucu, S. Onenc, and J. Yanik, "Production of Activated Carbon From Pine Cone and Evaluation of Its Physical, Chemical, and Adsorption Properties," *Energy & Fuels* 23, no. 4 (2009): 2197–2204, https://doi.org/10.1021/ef800510m.

22. Y. H. Fu, Y. F. Shen, Z. D. Zhang, X. L. Ge, and M. D. Chen, "Activated Bio-Chars Derived From Rice Husk via One- and Two-Step KOH-Catalyzed Pyrolysis for Phenol Adsorption," *Science of the Total Environment* 646 (2019): 1567–1577, https://doi.org/10.1016/j.scitotenv.2018.07.423.

23. E. Q. Ding, J. Q. Jiang, Y. Lan, et al., "Optimizing Cd2+ Adsorption Performance of KOH Modified Biochar Adopting Response Surface Methodology," *Journal of Analytical and Applied Pyrolysis* 169 (2023): 105788, https://doi.org/10.1016/j.jaap.2022.105788.

24. T. F. Chyad, R. F. C. Al-Hamadani, Z. A. Hammood, and G. A. Ali, "Removal of Zinc (II) Ions From Industrial Wastewater by Adsorption on to Activated Carbon Produced From Pine Cone," *Materials Today Proceedings* 80, no. 3 (2023): 2706–2711. https://doi.org/10.1016/j.matpr.2021.07.016.

25. M. Taheran, M. Naghdi, S. K. Brar, et al., "Adsorption Study of Environmentally Relevant Concentrations of Chlortetracycline on Pinewood Biochar," *Science of the Total Environment* 571 (2016): 772–777, https://doi.org/10.1016/j.scitotenv.2016.07.050.

26. N. E. Williams, O. A. Oba, and N. P. Aydinlik, "Modification, Production, and Methods of KOH-Activated Carbon," *ChemBioEng Reviews* 9, no. 2 (2022): 164–189, https://doi.org/10.1002/cben.202100030.

27. A. Pal, K. Uddin, K. Thu, et al. "Synthesis of High Grade Activated Carbons From Waste Biomass," *Encyclopedia of Renewable and Sustainable Materials* 4 (2020): 584. https://doi.org/10.1016/B978-0-12-803581-8.11341-4.

28. O. Paunovic, S. Pap, S. Maletic, M. A. Taggart, N. Boskovic, and M. Turk Sekulic, "Ionisable Emerging Pharmaceutical Adsorption onto Microwave Functionalised Biochar Derived From Novel Lignocellulosic

Waste Biomass," *Journal of Colloid and Interface Science* 547 (2019): 350–360, https://doi.org/10.1016/j.jcis.2019.04.011.

29. G. V. Nunell, M. E. Fernandez, P. R. Bonelli, and A. L. Cukierman, "Nitrate Uptake Improvement by Modified Activated Carbons Developed From Two Species of Pine Cones," *Journal of Colloid and Interface Science* 440 (2015): 102–108, https://doi.org/10.1016/j.jcis.2014.10.058.

30. H. T. Jiang, X. Li, J. N. Bai, W. Y. Pan, Z. Y. Luo, and Y. J. Dai, "Removal of Ciprofloxacin Lactate by Phosphoric Acid Activated Biochar: Urgent Consideration of New Antibiotics for Human Health," *Chemical Engineering and Science* 283 (2024): 119403, https://doi.org/10.1016/j.ces.2023.119403.

31. R. F. Chen, L. Q. Li, Z. Liu, et al., "Preparation and Characterization of Activated Carbons From Tobacco Stem by Chemical Activation," *Journal of the Air & Waste Management Association* 67, no. 6 (2017): 713–724, https://doi.org/10.1080/10962247.2017.1280560.

32. J. B. Ouyang, J. Chen, W. Q. Chen, L. M. Zhou, D. Cai, and C. Ren, "H3PO4 Activated Biochars Derived From Different Agricultural Biomasses for the Removal of Ciprofloxacin From Aqueous Solution," *Particuology* 75 (2023): 217–227, https://doi.org/10.1016/j.partic.2022.07.016.

33. R. Natarajan, K. Banerjee, P. Senthil, et al., "Performance Study on Adsorptive Removal of Acetaminophen From Wastewater Using Silica Microspheres: Kinetic and Isotherm Studies," *Chemosphere* 272 (2021): 129896, https://doi.org/10.1016/j.chemosphere.2021.129896.

34. H. Yu, L. Gu, L. Chen, H. Wen, D. Zhang, and H. Tao, "Activation of Grapefruit Derived Biochar by Its Peel Extracts and Its Performance for Tetracycline Removal," *Bioresource Technology* 316 (2020): 123971, https://doi.org/10.1016/j.biortech.2020.123971.

35. T. T. Nguyen, H. H. Chen, T. H. To, et al., "Development of Biochars Derived From Water Bamboo (Zizania Latifolia) Shoot Husks Using Pyrolysis and Ultrasound-Assisted Pyrolysis for the Treatment of Reactive Black 5 (RB5) in Wastewater," *Water* 13, no. 12 (2021): 1615, https://doi.org/10.3390/w13121615.

36. M. F. Idham, O. Falyouna, R. Eljamal, I. Maamoun, and O. Eljamal, "Chloramphenicol Removal From Water by Various Precursors to Enhance Graphene Oxide–Iron Nanocomposites," *Journal of Water Process Engineering* 50 (2022): 103289, https://doi.org/10.1016/j.jwpe.2022.103289.

37. R. Chandrasekar, H. K. Rajendran, V. P. V, and S. Narayanasamy, "Valorization of Sawdust by Mineral Acid Assisted Hydrothermal Carbonization for the Adsorptive Removal of Bisphenol A: A Greener Approach," *Chemosphere* 303 (2022): 135171. https://doi.org/10.1016/j.chemosphere.2022.135171.

38. J. Yang, G. Ji, Y. Gao, et al., "High-yield and High-Performance Porous Biochar Produced From Pyrolysis of Peanut Shell With Low-Dose Ammonium Polyphosphate for Chloramphenicol Adsorption," *Journal of Cleaner Production* 264 (2020): 121516, https://doi.org/10.1016/j.jclepro.2020.121516.

39. X. Zhu, Y. Gao, Q. Yue, Y. Song, B. Gao, and X. Xu, "Facile Synthesis of Hierarchical Porous Carbon Material by Potassium Tartrate Activation for Chloramphenicol Removal," *Journal of the Taiwan Institute of Chemical Engineers* 85 (2018): 141–148, https://doi.org/10.1016/j.jtice.2018.01.025.

40. J. Dai, J. He, A. Xie, et al., "Novel Pitaya-Inspired Well-Defined Core–Shell Nanospheres With Ultrathin Surface Imprinted Nanofilm From Magnetic Mesoporous Nanosilica for Highly Efficient Chloramphenicol Removal," *Chemical Engineering Journal* 284 (2016): 812–822, https://doi.org/10.1016/j.cej.2015.09.050.

41. Y. Wu, Q. Yue, Z. Ren, and B. Gao, "Immobilization of Nanoscale Zero-Valent Iron Particles (nZVI) With Synthesized Activated Carbon for the Adsorption and Degradation of Chloramphenicol (CAP)," *Journal of Molecular Liquids* 262 (2018): 19–28, https://doi.org/10.1016/j.molliq.2018.04.032.

42. R. Zhang, Z. Zhou, A. Xie, et al., "Preparation of Hierarchical Porous Carbons From Sodium Carboxymethyl Cellulose via Halloysite Template Strategy Coupled With KOH-Activation for Efficient Removal of Chloramphenicol," *Journal of the Taiwan Institute of Chemical Engineers* 80 (2017): 424–433, https://doi.org/10.1016/j.jtice.2017.07.032.

43. L. Qin, Z. Zhou, J. Dai, et al., "Novel N-Doped Hierarchically Porous Carbons Derived From Sustainable Shrimp Shell for High-Performance Removal of Sulfamethazine and Chloramphenicol," *Journal of the Taiwan Institute of Chemical Engineers* 62 (2016): 228–238, https://doi.org/10.1016/j.jtice.2016.02.009.

44. C. Zheng, H. Zheng, C. Hu, et al., "Structural Design of Magnetic Biosorbents for the Removal of Ciprofloxacin From Water," *Bioresource Technology* 296 (2020): 122288, https://doi.org/10.1016/j.biortech.2019.122288.

45. M. Li, Y. Liu, S. Liu, et al., "Cu(II)-influenced Adsorption of Ciprofloxacin From Aqueous Solutions by Magnetic Graphene Oxide/Nitrilotriacetic Acid Nanocomposite: Competition and Enhancement Mechanisms," *Chemical Engineering Journal* 319 (2017): 219–228, https://doi.org/10.1016/j.cej.2017.03.016.

46. O. Falyouna, M. F. Idham, I. Maamoun, et al., "Promotion of Ciprofloxacin Adsorption From Contaminated Solutions by Oxalate Modified Nanoscale Zerovalent Iron Particles," *Journal of Molecular Liquids* 359 (2022): 119323. https://doi.org/10.1016/j.molliq.2022.119323.

47. L. C. Dong, H. H. Ngo, W. S. Guo, et al., "Feasibility Study on A New Pomelo Peel Derived Biochar for Tetracycline Antibiotics Removal in Swine Wastewater," *Science of the Total Environment* 720 (2020): 137662. https://doi.org/10.1016/j.scitotenv.2020.137662.

48. L. M. Nguyen, N. T. T. Nguyen, T. T. T. Nguyen, T. T. Nguyen, D. T. C. Nguyen, and T. T. Tran, "Occurrence, Toxicity and Adsorptive Removal of the Chloramphenicol Antibiotic in Water: A Review," *Environmental Chemistry Letters* 20, no. 3 (2022): 1929–1963, https://doi.org/10.1007/s10311-022-01416-x.